

Conditional Video Generation for Effective Video Compression

Fangqiu Yi, Jingyu Xu, Jiawei Shao, Chi Zhang, Xuelong Li*.

{yifq1, xujy70, shaojw2, zhangc120}@chinatelecom.cn, xuelong_li@ieee.org
Institute of Artificial Intelligence (TeleAI), China Telecom

Abstract

Traditional and neural video compression methods often struggle at ultra-low bitrates, yielding video content with poor perceptual quality characterized by blurring, blocking, and color shifts. This limitation stems from their focus on pixel-level accuracy rather than extracting critical information essential for human visual perception. To overcome this limitation, we propose a novel video compression framework that reframes video compression as a conditional generation task, where a generative model synthesizes video from sparse yet informative signals. Our approach introduces three key modules: (1) Multi-granular conditioning that captures both static scene structure and dynamic spatio-temporal cues; (2) Compact representations designed for efficient transmission without sacrificing semantic richness; (3) Multi-condition training with modality dropout and role-aware embeddings, which prevent over-reliance on any single modality and enhance robustness. Extensive experiments show that our method significantly outperforms both traditional and neural codecs on perceptual quality metrics such as Fréchet Video Distance (FVD) and LPIPS, especially under high compression ratios.

Introduction

The exponential growth of video content across streaming platforms, social networks, teleconferencing, and augmented reality applications has created unprecedented demand for effective compression techniques. Current video compression standards, including H.266/VVC (Zhang et al., 2020) and AV1 (Chen et al., 2020), have achieved substantial improvements through decades of engineering refinement, employing hybrid coding strategies that combine motion estimation, transform coding, and entropy modeling. However, these approaches rely on largely handcrafted components within rigid codec architectures, limiting their adaptability to diverse application requirements.

Most traditional and neural compression pipelines operate under a fundamental assumption: the pursuit of pixel-level fidelity to ensure reconstructed frames match the original input as closely as possible. While this approach suits applications requiring exact reproduction—such as scientific imaging or professional video editing—we argue that strict fidelity is often unnecessary for perceptual consumption scenarios. In applications like user-generated content,

entertainment streaming, or virtual conferencing, perceptual consistency—visual coherence aligned with human perception—matters more than exact pixel reconstruction. Relaxing pixel-perfect accuracy requirements creates opportunities for aggressive compression while enabling new trade-offs between bitrate and perceptual quality. Data-driven approaches have emerged as promising alternatives to traditional codecs. Recent advances in neural image and video compression leverage encoder-decoder architectures and learned entropy models to achieve competitive rate-distortion performance. However, most methods remain constrained by deterministic reconstruction requirements and often exhibit suboptimal perceptual quality, particularly at low bitrates, manifesting as blurring, blocking artifacts, and color degradation.

Concurrently, generative models—especially diffusion models—have demonstrated state-of-the-art performance in image and video synthesis. This paradigm shifts focus from encoding pixel-level residuals to achieving content-faithful reconstruction under strict bitrate constraints by leveraging the strong priors of generative models and compact spatio-temporal guidance. While existing methods (Zhang et al., 2025; Wan, Zheng, and Fan, 2024; Wu et al., 2023) model spatio-temporal information via textual prompts, keyframes, or basic visual cues, we contend these representations are insufficient for high-fidelity video reconstruction. This limitation confines their applicability to narrow domains—such as human-face video (Chen et al., 2024), human-body video (Wang et al., 2023a, 2022), or small motion video (Yin et al., 2024) — where scene complexity remains constrained.

We explore this question through a diffusion-based compression framework that introduces three core innovations. First, we employ multi-granular signals that capture both static scene structure such as auto selected keyframes and semantic descriptions, and dynamic information including human motion, optical flow, and panoptic segmentation. Second, we design compact, transmission-efficient representations for these signals that serve as minimal yet perceptually informative inputs to the decoder. Third, we develop a multi-condition training strategy that incorporates signal dropout and role-aware embeddings, enabling the model to remain robust even when certain signals are unavailable or degraded.

We evaluate our method on standard video benchmarks using perceptual metrics including Fréchet Video Distance (FVD) and LPIPS. Results demonstrate substantial improvements over both traditional and learning-based codecs in perceptual quality, particularly at high compression ratios. These findings suggest that conditional generative models offer a promising paradigm for perception-centric video compression, where semantic compactness and visual plausibility supersede strict pixel accuracy.

To summarize, our main contributions are threefold:

- First, we design an efficient and modular compression framework, incorporating multi-granular conditioning and compact, transmission-friendly representations to guide reconstruction with minimal overhead.
- Second, we deploy a multi-condition training strategy enabling the model to remain robust even when certain signals are unavailable or degraded.
- Third, we demonstrate state-of-the-art perceptual performance on standard benchmarks, significantly outperforming traditional and neural codecs under high compression ratios, as measured by FVD and LPIPS.

Related Work

Video Compression

Video compression aims to reduce redundant information in video sequences while preserving critical visual content, enabling efficient storage and transmission across applications such as streaming services, video conferencing, and surveillance. With the success of deep learning in image compression (Mishra, Singh, and Singh, 2022), neural video compression has emerged as a prominent research area, leveraging neural networks to optimize rate-distortion trade-offs. Residual coding-based approaches (Choi and Bajić, 2019) generate predicted frames from previously decoded ones and encode the residual between predicted and current frames. However, their reliance on simple subtraction for inter-frame redundancy reduction leads to suboptimal performance. Lu et al. (Li, Li, and Lu, 2021) pioneered this direction by replacing traditional codec modules with neural networks in an end-to-end framework. The DCVC series (Li, Li, and Lu, 2021) exemplifies this paradigm, with DCVC-DC (Li, Li, and Lu, 2023) and DCVC-FM (Li, Li, and Lu, 2024) outperforming traditional codecs like ECM (Karadimitriou, 1996). While these neural video compression methods have made significant strides in improving rate-distortion performance as measured by pixel-level metrics, they often overlook the perceptual quality of the reconstructed videos, which is crucial for human viewing experience. This gap between pixel-level metrics and perceptual quality led Blau et al. (Blau and Michaeli, 2019) to highlight a “rate-distortion-perception” trade-off, spurring research into perceptual video compression.

Conditional Video Generation

Conditional video generation aims to synthesize videos adhering precisely to external conditions (appearance, layout, motion) while maintaining spatiotemporal consistency.

Early methods extended image diffusion models with text guidance, enabling creative generation but lacking fine-grained detail and motion control. Subsequent approaches incorporated stronger conditions: Image animation methods used initial frames but often produced static results. Methods using low-level dense signals (e.g., depth or edge sequences: Gen-1 (Esser et al., 2023), ControlVideo (Zhao et al., 2025), VideoComposer (Wang et al., 2023b)) improved control but proved impractical. Object trajectory or layout control emerged via strokes (DragNUWA (Yin et al., 2023)), coordinates (MotionCtrl (Wang et al., 2024b)), or bounding boxes. Training-based trajectory methods (TrackGo (Zhou et al., 2025)) were costly with limited gains, while training-free attention manipulation (FreeTraj (Qiu et al., 2024)) suffered inaccuracies. Critically, existing methods remain fragmented: each control modality typically requires specialized inputs or architectural changes, highlighting the need for unified, adaptable frameworks.

Diffusion Models for Video Compression

Diffusion-based compression has advanced rapidly in the image domain, laying groundwork for video applications. Wu et al. (Wu et al., 2023) transmitted sketches and text descriptions to guide diffusion-based reconstruction, while Careil et al. (Careil et al., 2023) used vector-quantized latents and captions for decoding. Relic et al. (Relic et al., 2025) optimized efficiency by framing quantization noise removal as a denoising task with adaptive steps. However, extending these advances to video faces key challenges: integrating foundational diffusion models into existing video coding paradigms (e.g., conditional coding) without disrupting efficiency, mitigating slow inference, and enabling multi-bitrate support for varying latent distortion levels. To address these, this work focuses on diffusion-based video compression, emphasizing dynamic and static condition controls to balance compression ratio and perceptual quality. By harmonizing these conditions, the proposed method enhances reconstruction fidelity across bitrates while preserving coding efficiency—bridging the gap between diffusion-based image compression success and unmet needs in video coding.

Method

In this section, we formally introduce our proposed video compression framework, which consists of three key stages, as illustrated in Figure 1. Each stage is designed to extract, compress, and reconstruct video content in a perceptually consistent and bandwidth-efficient manner.

Keyframe Selection and Clip Segmentation. The input video is first processed by a keyframe selection module, which partitions it into sequential, non-overlapping clips. For each clip, the first and last frames are selected as keyframes, serving as spatial anchors for subsequent reconstruction. These keyframes also act as natural segmentation points, enabling each clip to be independently encoded and decoded.

Conditional Feature Extraction and Compression. For the intermediate (non-key) frames within each clip, we ex-

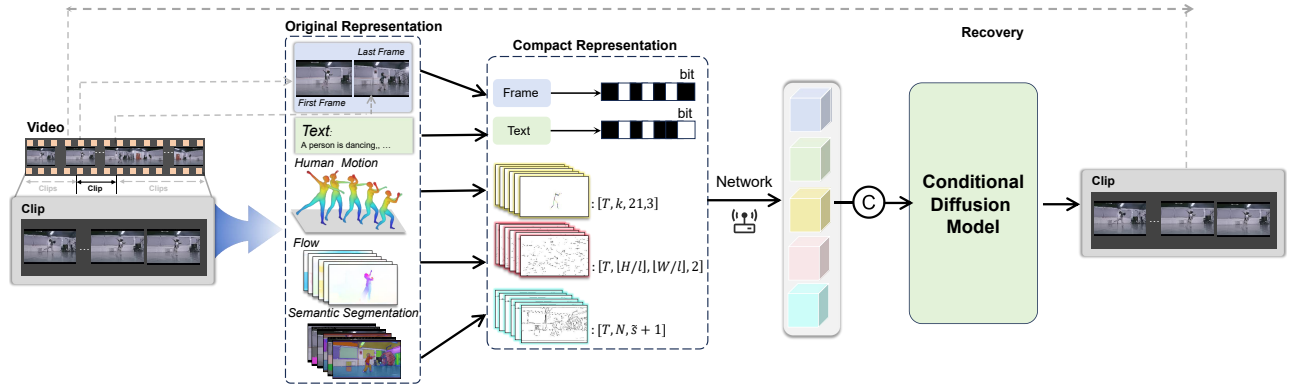


Figure 1: Our framework processes input videos through three sequential stages: First, a keyframe selection module partitions the video into consecutive clips. Second, clip-specific conditions are compressed—the first frame, last frame, and textual descriptions via entropy coding while segmentation sequences, human motion data, and optical flow are converted to compact representations. Finally, at the decoder, a conditional diffusion model reconstructs each clip using all decompressed conditions to generate the output video.

tract a set of multi-granular conditional features that capture complementary aspects of the visual content. These include semantic captions (textual descriptions of the scene), panoptic segmentation maps (spatial structure), human motion sequences, and optical flow (temporal dynamics). The extracted features are then compressed into a compact representation suitable for transmission, preserving the essential cues needed for high-quality reconstruction while minimizing bitrate.

Conditional Frame Generation at the Decoder. Each clip is transmitted as a combination of compressed keyframes and compact conditional representations. At the decoder, we employ a pre-trained multi-conditional diffusion model to reconstruct the intermediate frames by jointly conditioning on the received keyframes and auxiliary signals. This generative process ensures both spatial fidelity and temporal coherence across the reconstructed video sequence.

We now provide detailed descriptions of each component in the following subsections.

1. Keyframe Selection and Clip Segmentation

Our keyframe selection strategy employs dual-criterion detection to balance compression efficiency and reconstruction quality. Formally, given video sequence $\mathcal{V} = \{f_1, f_2, \dots, f_T\}$ with T frames, we identify keyframes through:

- (i) **Shot boundary detection:** Frame f_i is selected when identified as a shot transition frame using TransNetV2 (Souček and Lokoč, 2020). We compute shot transition probability $p_i = \mathcal{T}(f_i)$ where \mathcal{T} denotes the pretrained TransNetV2 model, and designate f_i as a keyframe when $p_i > 0.5$.
- (ii) **Fixed-interval sampling:** Frame f_i is selected if $i - i_{\text{prev}} \geq w$, where w is a tunable hyperparameter and i_{prev} denotes the previous keyframe index. Smaller w values increase keyframe density (improving reconstruction qual-

ity at higher bitrates) while larger w reduces transmission overhead.

2. Conditional Feature Extraction

Empirical studies have established that, spatiotemporal control signals significantly enhance motion dynamics, spatial alignment, and temporal consistency - critical factors for perceptual fidelity in video reconstruction. Besides the textual descriptions obtained through VLLM, we select three complementary conditional representations whose compact forms balance reconstruction quality against transmission bandwidth.

Segmentation Sequences

Segmentation sequences provide crucial geometric scaffolding by preserving object boundaries and spatial relationships across frames. This explicit structural prior prevents shape distortion during generation and maintains consistent object interactions throughout temporal transitions. We extract per-frame panoptic segmentation map using Mask2Former (Cheng et al., 2021). To achieve high compression, we first extract its external contour using border tracing, and then approximate each contour with n -th order Bézier curves:

$$B(t) = \sum_{i=0}^n \binom{n}{i} (1-t)^{n-i} t^i P_i, \quad t \in [0, 1]$$

where P_i are optimized control points. Finally, we retain only the N longest contours per frame. Fig. 3(a) shows the original segmentation map and the fitting results obtained with different values of N , where 8th-order Bézier curve is applied. This compact representation preserves essential object topology while largely reducing storage since only the Bézier parameters need to be saved.

Human Motion Representation

Human motion sequences are essential for human-centric videos (Zhang et al., 2024) since it significantly reduces ar-

Algorithm 1 Keyframe-based Clip Segmentation

Require: Video frames $\mathcal{V} = \{f_1, f_2, \dots, f_T\}$,
Hyperparameter w ,
Shot detector \mathcal{T}

Ensure: Clips $\mathcal{C} = \{\text{start}_m, \text{end}_m\}_{m=1}^M$

- 1: $\mathcal{K} \leftarrow \{0\}$ ▷ Initialize with first frame
- 2: $\text{last_key} \leftarrow 0$
- 3: $\text{prev_type} \leftarrow \text{null}$
- 4: **for** $i \leftarrow 1$ **to** T **do**
- 5: **if** $(i - \text{last_key}) \geq w$ **or** $\mathcal{T}(f_i) > 0.5$ **then**
- 6: $\mathcal{K} \leftarrow \mathcal{K} \cup \{i\}$
- 7: **if** $(i - \text{last_key}) \geq w$ **then**
- 8: $\text{prev_type} \leftarrow \text{interval}$
- 9: **else**
- 10: $\text{prev_type} \leftarrow \text{shot}$
- 11: **end if**
- 12: $\text{last_key} \leftarrow i$
- 13: **end if**
- 14: **end for**
- 15: $\mathcal{K} \leftarrow \mathcal{K} \cup \{T\}$ ▷ Add last frame
- 16: $\mathcal{C} \leftarrow \emptyset$
- 17: $\text{keys} \leftarrow \text{SORT}(\mathcal{K})$ ▷ Sorted keyframe indices
- 18: **for** $j \leftarrow 1$ **to** $|\text{keys}| - 1$ **do**
- 19: $s \leftarrow \text{keys}[j - 1]$
- 20: $e \leftarrow \text{keys}[j]$
- 21: **if** $\text{prev_type} = \text{shot}$ **then**
- 22: $s \leftarrow s + 1$ ▷ Offset for shot boundary
- 23: **end if**
- 24: $\mathcal{C} \leftarrow \mathcal{C} \cup \{[s, e]\}$
- 25: $\text{prev_type} \leftarrow \text{type of } \text{keys}[j]$
- 26: **end for**

tifacts in articulated movements and maintains natural temporal coherence during complex actions like walking or dancing. We represent human motion using 3D SMPL sequences (Loper et al., 2015). Then, we select 21 joints that represents human kinetics and project those 3D joints to 2D image-coordinates. By calculating the proportion of the area occupied by 2D joints in the image coordinates, we set different thresholds to filter out small human poses. Fig. 3(b) shows the human motion results obtained with different area-threshold ξ . The 2D joints coordinates are transmitted over the network.

Optical Flow Representation

Optical flow fields explicitly encode dense displacement vectors between pixels, providing critical motion guidance. We compute optical flow using RAFT (Teed and Deng, 2020). However, the cost of transmitting pixel-level optical flow is prohibitively expensive. We believe that the representation of optical flow should be based on blocks of pixels rather than individual pixels. Specifically, we define sampling stride l (hyperparameter controlling compression ratio) and then sample flow vectors at regular intervals.

$$\mathcal{G} = \{\mathcal{G}(x, y) \mid x = \lfloor i \cdot l \rfloor, y = \lfloor j \cdot l \rfloor\}$$

where $i = 1, 2, \dots, \lfloor H/l \rfloor$, $j = 1, 2, \dots, \lfloor W/l \rfloor$, \mathcal{G} is the extracted optical flow map.

Under large sampling strides, bilinear interpolation produces significant errors in recovered optical flow fields. Therefore, we employ a flow-arrow visualization approach where arrow direction indicates motion orientation at sampled points and arrow length represents flow magnitude. Fig. 3(c) demonstrates this flow visualization across different sampling strides.

Compression Calculation

For a clip, the first and last frames are encoded into a bit-stream using a state-of-the-art image compression method, such as LIC (Li et al., 2025), along with text, with a size set to Q KB. The representations of the remaining three conditions are directly encoded in numeric form, with each number represented using bfloat16 (2 Bytes). The compressed bitrate (KBps) of our framework is calculated per video clip as:

$$R = \frac{Q \cdot \text{fps}}{T} + \frac{2 \cdot \text{fps}}{1024} \cdot \left[\phi(\xi) \cdot 21 \cdot 2 + 2 \left\lfloor \frac{H}{l} \right\rfloor \left\lfloor \frac{W}{l} \right\rfloor + 2N(n+1) \right] \quad (1)$$

- Q : Size of compressed first frame and last frame + text (KB)
- T : Clip length
- fps : Frame rate (frames/sec) of the clip
- k : The number of people pose remaining under threshold $\phi(\xi)$
- H, W : Frame dimensions (pixels)
- l : Flow sampling stride
- N : The number of Bézier curves
- n : Order of Bézier curve (default: 8)

3. Conditional Frame Generation at Decoder

Our conditional diffusion model is built upon the pre-trained FL2V diffusion model WAN2.1 (Wan, 2025). Firstly, the condition signals, i.e. segmentation/human motion/optical flow are convert to dense visual modalities $V = \{V_{\text{seg}}, V_{\text{motion}}, V_{\text{flow}}\} \in R^{T*H*W*3}$, as shown in Fig. 3. Given the paried visual modalities, we first encode them into a latent space using a pretrained 3D causal VAE encoder ϵ .

$$x_m = \epsilon(V_m), m \in \{\text{flow}, \text{motion}, \text{seg}\}$$

During training, a key challenge arises from modality entanglement: the model often over-relies on dominant conditions (e.g., segmentation) while neglecting others. To enforce balanced utilization, We apply **random dropout** for each condition with a dropout ratio of 0.3. For any condition subjected to dropout, its visual representation is replaced with a zero-valued (all-black) image sequence.

Meanwhile, random dropout introduces an another problem: **role ambiguity**. Under extreme transmission conditions, certain conditioning signals may be lost or become incomplete, such as the absence of pose control. However, the model is unable to distinguish whether the missing condition

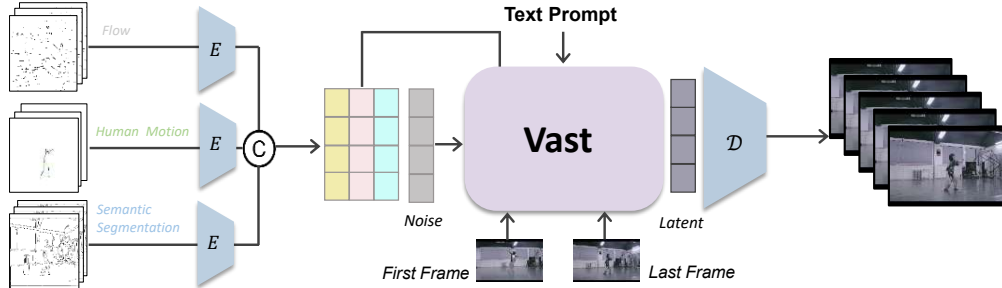


Figure 2: Our diffusion model converts optical flow, segmentation, and motion into visual modalities, encodes them via VAE, and concatenates the latent codes with noise as input to the diffusion backbone.

results from accidentally absent conditions or from dropout-induced zeros. To address this, we introduce an adaptive control strategy that dynamically assigns roles to different modalities. This idea is first introduced by OmniVDiff (Xi et al., 2025) to distinguish whether the input is intended for joint generation or merely as conditioning information. Distinct from their objective, we introduce a modality embedding e_m that differentiates between the roles of *dropout* (e_d) and *conditioning* (e_c), which can be directly added to the latent space.

$$x_m = \bar{x}_m + [\delta_m e_d + (1 - \delta_m) e_c], \quad (2)$$

where δ_m is a binary indicator taking values 0 or 1, specifying whether dropout is applied to m :

$$\begin{aligned} \delta_m = 1 &\Rightarrow \text{the dropout offset } e_d \text{ is used,} \\ \delta_m = 0 &\Rightarrow \text{the conditioning offset } e_c \text{ is used.} \end{aligned}$$

Finally, we concatenate x_m along the channel dimension with the latent noise, forming the input of the diffusion transformer. We freeze the majority of the diffusion model’s parameters and perform efficient adaptation via Low-Rank Adaptation (LoRA) (Hu et al., 2022).

This strategy enables flexible and efficient control, allowing the model to remain robust even when certain signals are unavailable.

Experiments

For training the multi-condition diffusion model, we employ a curated subset of 20,000 diverse video sequences sampled from Koala-36M (Wang et al., 2024a). To evaluate the performance of our method and state-of-the-art (SOTA) methods on the video compression task, we conduct a series of experiments and empirical studies on public datasets including HEVC Class B, C (Boyce et al., 2010) as well as UVG (Mercat, Viitanen, and Vanne, 2020) and MCL-JCV (Wang et al., 2016), following (Wan, Zheng, and Fan, 2024) and T-GVC (Wang et al., 2025). Furthermore, to address the limited scene coverage in open-source benchmarks, we conduct rigorous cross-dataset evaluation on our curated internet-sourced video corpus. Extensive experiments validating our method’s generalization capability across diverse real-world scenarios are provided in the supplementary material.

Experimental Settings

Evaluation Metrics. We use two commonly used metrics for evaluation: **Fréchet Video Distance (FVD)** and **Learned Perceptual Image Patch Similarity (LPIPS)**, as they better align with human perception compared to traditional measures such as PSNR and SSIM. Lower FVD and LPIPS at the same bitrate represent better performance.

Baselines. To demonstrate the effectiveness of the framework, we compare the proposed framework with both traditional video compression standards, H.264, H.265, H.266, and SOTA video compression methods: (1) traditional video compression methods (H.264 (Wiegand et al., 2003), H.265 (Sullivan et al., 2012), H.266 (Bross et al., 2021)); (2) neural video compression methods (DCVC-DC (Li, Li, and Lu, 2023), DCVC-FM (Li, Li, and Lu, 2024), DCVC-RT (Jia et al., 2025)); (3) diffusion-based video compression methods (T-GVC).

Level	Segmentation	Human Motion	Optical Flow
Level 0	N/A	N/A	N/A
Level 1	$N = 10$	$\xi = 1/5$	$l = 128$
Level 2	$N = 20$	$\xi = 1/8$	$l = 96$
Level 3	$N = 30$	$\xi = 1/10$	$l = 64$

Table 1: Different compression settings.

Compression Settings. To demonstrate the effectiveness of our framework comprehensively, we design multiple compression settings, as shown in Table 1. Specifically, for Level 0, we only use the first and the last frame of the clip, with no additional conditions provided. During training, we randomly select one configuration from multiple compression settings to process the training data, enabling a single model to simultaneously handle inputs with different settings.

Hyperparameter Settings. For a fair comparison, all methods are implemented with PyTorch 2.5 in Python 3.9.13 and learned with Adam optimizer (Kingma and Ba, 2017). We conduct our experiments on a single Linux server with 2 Intel(R) Xeon(R) CPU Platinum 8558 @2.10 GHz, 2 TB RAM, and 8 NVIDIA H100 (80 GB of graphic memory each). We fine-tune the pre-trained Wan2.1-14B for 3 epochs with a learning rate of 2×10^{-5} and a batch size of 8. We

Method	HEVC Class B		HEVC Class C		UVG		MCL-JCV	
	FVD (\downarrow)	LPIPS (\downarrow)	FVD (\downarrow)	LPIPS (\downarrow)	FVD (\downarrow)	LPIPS (\downarrow)	FVD (\downarrow)	LPIPS (\downarrow)
H.264 (Wiegand et al., 2003)	2738	0.8283	3022	0.7724	4252	0.8274	4844	0.7139
H.265 Sullivan et al. (2012)	1327	0.4941	1452	0.4833	1688	0.4052	1030	0.3667
H.266 (Bross et al., 2021)	1022	0.4038	1273	0.4543	1052	0.2834	973	0.3217
DCVC-DC (Li, Li, and Lu, 2023)	892	0.3821	1135	0.4327	992	0.2742	887	0.3152
DCVC-FM (Li, Li, and Lu, 2024)	837	0.3672	1079	0.4186	968	0.2689	849	0.3103
DCVC-RT (Jia et al., 2025)	783	0.3543	1029	0.4058	947	0.2635	811	0.3068
T-GVC (Wang et al., 2025)	-	0.3512	-	0.3642	-	0.2212	-	0.3145
Ours	597	0.2813	402	0.2625	571	0.2208	515	0.2926

Table 2: The overall performance of different methods on the test sets (BPP = 0.0066). Here, we report the FVD and LPIPS among actual videos and predictions generated by different methods. The best results are highlighted in **bold**.

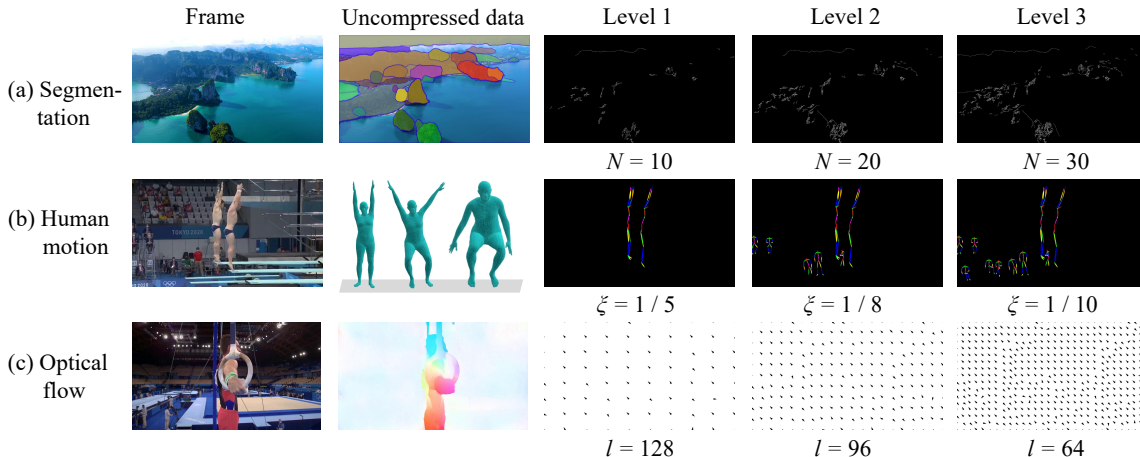


Figure 3: Visualization of optical flow, human motion, and segmentation representations alongside their compact forms at varying bitrate thresholds.

tuned the parameters of all methods over the validation set. We set rank (r) and alpha (α) to 16 for LoRA.

Overall Performance

Table 2 summarizes the performance of all models on Level 1 (BPP = 0.0066). Please note that since T-GVC has not released its codebase, we directly use the performance reported in the paper (Wang et al., 2025). Fig. 4 summarizes the overall performance of all models on other levels (Level 0: BPP = 0.0024, Level 2: BPP = 0.0099, Level 3: BPP = 0.0183). Here, we make the following observations.

First, our diffusion-based video compression framework (conditioned on human motion, canny edges, and optical flow) outperforms traditional codecs (H.264/H.265/H.266) and neural compression baselines (e.g., DCVC-RT) in all bitrate settings. Quantitative metrics (FVD and LPIPS) show improvements of 15–30%, particularly in extreme low bitrate settings, confirming that the generated videos better preserve perceptual quality, avoiding blocking artifacts (common in traditional codecs) and over-smoothed textures (typical of neural methods).

Second, while higher compression ratios lead to lower objective scores, the generative nature of diffusion ensures graceful degradation in perceptual quality. Even at level 1

compression where bpp is less than 0.007, key motion and semantics remain recognizable (see visualized results), making the method viable for bandwidth-constrained applications (e.g., mobile streaming, surveillance).

Last, traditional codecs like H.264 fail to produce results at extreme low bitrates, exhibiting severe blocking artifacts and temporal inconsistency. In contrast, our method maintains coherent motion and sharp edges even at Level 1 (BPP = 0.0066), demonstrating superior robustness across bitrates.

Ablation Study

To validate the necessity of our core innovations, stochastic modality dropout and role-aware embeddings, we conduct ablation experiments with a baseline model, which is trained without both modality dropout and role-aware embeddings. We perform the study by systematically removing individual modalities—segmentation sequences (Seg), human motion (Motion), and optical flow (Flow). It worth noting that, when modality is ablated, its visual representation is replaced with a zero-valued (all-black) image sequence. Meanwhile, for our model, the modality embedding e_m is assigned to the dropout role e_d , which then will be added in the latent space. We have two observations: Firstly, as shown in Fig. 5(c), when one modality is missing, baseline

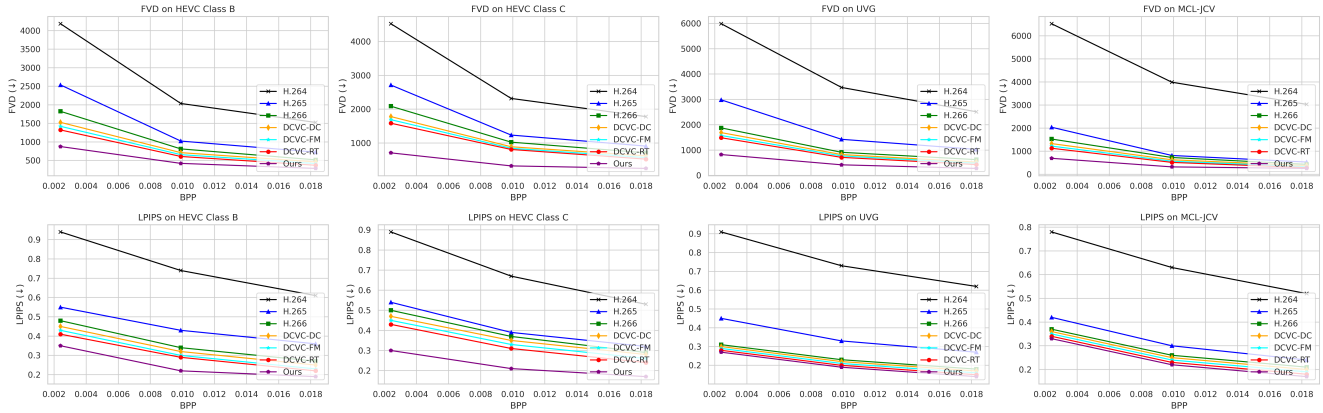


Figure 4: R-D (perception) performance with state-of-the-art models. **Upper:** FVD (\downarrow) on HEVC-B/C, UVG and MCL-JCV datasets; **Lower:** LPIPS (\downarrow) on HEVC-B/C, UVG and MCL-JCV datasets.

Table 3: The ablation study of condition settings on the UVG and MCL-JCV datasets at Level 1 (BPP = 0.0066). The best results are highlighted in **bold**.

Condition	UVG		MCL-JCV	
	FVD (\downarrow)	LPIPS (\downarrow)	FVD (\downarrow)	LPIPS (\downarrow)
w/o Seg	623	0.2481	577	0.3102
w/o Motion	605	0.2353	618	0.3369
w/o Flow	589	0.2308	542	0.3015
full model	571	0.2208	515	0.2926



Figure 5: Ablation study on role-aware embeddings.

model causes catastrophic failure and yields noise-like outputs. Secondly, as shown in Table 3, our model achieves best results across both datasets when all modalities are valid, while removing any single condition degrades the FVD.

The ablation experiments demonstrate that our multi-condition training paradigm not only prevents the model from over-relying on any single cue, but also enables the composition of arbitrary condition subsets at the decoder to faithfully emulate degradation patterns encountered in real-world scenarios.

Visualized Results

In this subsection, we present some visualized results to demonstrate the performance of our model and comparative methods intuitively.

Fig. 6 provides a qualitative comparison of video compression performance across different methods, specifically between Ours, H.264/H.265, and the Ground Truth. The selected sample illustrates that our method preserves seman-

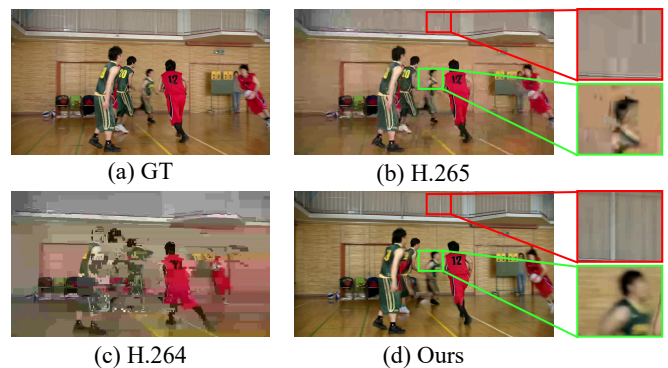


Figure 6: Visual comparison with SOTA codecs on the HEVC Class B set. We present the frame between original video, H.264/H.265, and our model. All predicted results are controlled to have a bpp of 0.0099 (Best viewed zoomed in and in color).

tic and structural details even at ultra low bitrates, whereas H.264 and H.265 exhibit significant compression artifacts including noticeable blurring effects.

Conclusion

This paper presents a video compression framework leveraging conditional diffusion models to achieve human-perception-aligned reconstruction at ultra-low bitrates. Despite these advances, limitations remain: The current decoding speed falls short of real-time requirements due to computational intensity in diffusion-based generation. To address this, we propose adopting *familiar model*—deploying homologous diffusion models of varying capacities—enabling automatic model switching based on decoder-side computational resources, inspired by AI Flow paradigms (An et al., 2025). Additionally, content-agnostic bitrate control via manual parameter tuning (e.g., l , N , ξ) limits adaptability. Future work will integrate content-understanding modules to dynamically optimize compression thresholds based on scene complexity and motion characteristics.

References

- An, H.; Hu, W.; Huang, S.; Huang, S.; Li, R.; Liang, Y.; Shao, J.; Song, Y.; Wang, Z.; Yuan, C.; Zhang, C.; Zhang, H.; Zhuang, W.; and Li, X. 2025. Ai flow: Perspectives, scenarios, and approaches.
- Blau, Y., and Michaeli, T. 2019. Rethinking lossy compression: The rate-distortion-perception tradeoff. In *International Conference on Machine Learning*, 675–685. PMLR.
- Boyce, J. M.; Suehring, K.; Li, X.; and Seregin, V. 2010. Jvet-j1010: Jvet common test conditions and software reference configurations. *3rd. JCT-VC Meeting*.
- Bross, B.; Wang, Y.-K.; Ye, Y.; Liu, S.; Chen, J.; Sullivan, G. J.; and Ohm, J.-R. 2021. Overview of the versatile video coding (vvc) standard and its applications. *IEEE Transactions on Circuits and Systems for Video Technology* 31(10):3736–3764.
- Careil, M.; Muckley, M. J.; Verbeek, J.; and Lathuilière, S. 2023. Towards image compression with perfect realism at ultra-low bitrates. In *The Twelfth International Conference on Learning Representations*.
- Chen, Y.; Mukherjee, D.; Han, J.; Grange, A.; Xu, Y.; Parker, S.; Chen, C.; Su, H.; Joshi, U.; Chiang, C.-H.; et al. 2020. An overview of coding tools in av1: the first video codec from the alliance for open media. *APSIPA Transactions on Signal and Information Processing* 9:e6.
- Chen, B.; Chen, J.; Wang, S.; and Ye, Y. 2024. Generative face video coding techniques and standardization efforts: A review. In *2024 Data Compression Conference (DCC)*, 103–112.
- Cheng, B.; Misra, I.; Schwing, A. G.; Kirillov, A.; and Girshick, R. 2021. Masked-attention mask transformer for universal image segmentation. *arXiv*.
- Choi, H., and Bajić, I. V. 2019. Deep frame prediction for video coding. *IEEE Transactions on Circuits and Systems for Video Technology* 30(7):1843–1855.
- Esser, P.; Chiu, J.; Atighehchian, P.; Granskog, J.; and Germanidis, A. 2023. Structure and content-guided video synthesis with diffusion models. In *Proceedings of the IEEE/CVF international conference on computer vision*, 7346–7356.
- Hu, E. J.; Shen, Y.; Wallis, P.; Allen-Zhu, Z.; Li, Y.; Wang, S.; Wang, L.; and Chen, W. 2022. LoRA: Low-rank adaptation of large language models. In *International Conference on Learning Representations*.
- Jia, Z.; Li, B.; Li, J.; Xie, W.; Qi, L.; Li, H.; and Lu, Y. 2025. Towards practical real-time neural video compression. In *Proceedings of the IEEE/CVF Conference on Computer Vision and Pattern Recognition*.
- Karadimitriou, K. 1996. *Set redundancy, the enhanced compression model, and methods for compressing sets of similar images*. Louisiana State University and Agricultural & Mechanical College.
- Kingma, D. P., and Ba, J. 2017. Adam: A method for stochastic optimization.
- Li, H.; Li, S.; Dai, W.; Cao, M.; Kan, N.; Li, C.; Zou, J.; and Xiong, H. 2025. On disentangled training for non-linear transform in learned image compression. In *The Thirteenth International Conference on Learning Representations*.
- Li, J.; Li, B.; and Lu, Y. 2021. Deep contextual video compression. *Advances in Neural Information Processing Systems* 34:18114–18125.
- Li, J.; Li, B.; and Lu, Y. 2023. Neural video compression with diverse contexts. In *Proceedings of the IEEE/CVF Conference on Computer Vision and Pattern Recognition*, 22616–22626.
- Li, J.; Li, B.; and Lu, Y. 2024. Neural video compression with feature modulation. In *Proceedings of the IEEE/CVF Conference on Computer Vision and Pattern Recognition*, 26099–26108.
- Loper, M.; Mahmood, N.; Romero, J.; Pons-Moll, G.; and Black, M. J. 2015. Smpl: a skinned multi-person linear model. *ACM Trans. Graph.* 34(6).
- Mercat, A.; Viitanen, M.; and Vanne, J. 2020. Uvg dataset: 50/120fps 4k sequences for video codec analysis and development. In *Proceedings of the 11th ACM Multimedia Systems Conference, MMSys '20*, 297–302. New York, NY, USA: Association for Computing Machinery.
- Mishra, D.; Singh, S. K.; and Singh, R. K. 2022. Deep architectures for image compression: a critical review. *Signal Processing* 191:108346.
- Qiu, H.; Chen, Z.; Wang, Z.; He, Y.; Xia, M.; and Liu, Z. 2024. Freetraj: Tuning-free trajectory control in video diffusion models. *arXiv preprint arXiv:2406.16863*.
- Relic, L.; Azevedo, R.; Zhang, Y.; Gross, M.; and Schroers, C. 2025. Bridging the gap between gaussian diffusion models and universal quantization for image compression. In *Proceedings of the IEEE/CVF Conference on Computer Vision and Pattern Recognition*, 2449–2458.
- Souček, T., and Lokoč, J. 2020. Transnet v2: An effective deep network architecture for fast shot transition detection. *arXiv preprint arXiv:2008.04838*.
- Sullivan, G. J.; Ohm, J.-R.; Han, W.-J.; and Wiegand, T. 2012. Overview of the high efficiency video coding (hevc) standard. *IEEE Transactions on Circuits and Systems for Video Technology* 22(12):1649–1668.
- Teed, Z., and Deng, J. 2020. Raft: Recurrent all-pairs field transforms for optical flow. In *European Conference on Computer Vision*, 402–419. Cham: Springer International Publishing.
- Wan, R.; Zheng, Q.; and Fan, Y. 2024. M3-cvc: Controllable video compression with multimodal generative models.
- Wan, T. 2025. Wan: Open and advanced large-scale video generative models. *arXiv preprint arXiv:2503.20314*.
- Wang, H.; Gan, W.; Hu, S.; Lin, J. Y.; Jin, L.; Song, L.; Wang, P.; Katsavounidis, I.; Aaron, A.; and Kuo, C.-C. J. 2016. Mcl-jcv: A jnd-based h.264/avc video quality assessment dataset. In *2016 IEEE International Conference on Image Processing (ICIP)*, 1509–1513.

- Wang, R.; Mao, Q.; Wang, S.; Jia, C.; Wang, R.; and Ma, S. 2022. Disentangled visual representations for extreme human body video compression. In *2022 IEEE International Conference on Multimedia and Expo (ICME)*, 1–6.
- Wang, R.; Mao, Q.; Jia, C.; Wang, R.; and Ma, S. 2023a. Extreme generative human-oriented video coding via motion representation compression. In *2023 IEEE International Symposium on Circuits and Systems (ISCAS)*, 1–5.
- Wang, X.; Yuan, H.; Zhang, S.; Chen, D.; Wang, J.; Zhang, Y.; Shen, Y.; Zhao, D.; and Zhou, J. 2023b. Videocomposer: Compositional video synthesis with motion controllability. *Advances in Neural Information Processing Systems* 36:7594–7611.
- Wang, Q.; Shi, Y.; Ou, J.; Chen, R.; Lin, K.; Wang, J.; Jiang, B.; Yang, H.; Zheng, M.; Tao, X.; Yang, F.; Wan, P.; and Zhang, D. 2024a. Koala-36m: A large-scale video dataset improving consistency between fine-grained conditions and video content.
- Wang, Z.; Yuan, Z.; Wang, X.; Li, Y.; Chen, T.; Xia, M.; Luo, P.; and Shan, Y. 2024b. Motionctrl: A unified and flexible motion controller for video generation. In *ACM SIGGRAPH 2024 Conference Papers*, 1–11.
- Wang, Z.; Man, H.; Li, W.; Wang, X.; Fan, X.; and Zhao, D. 2025. T-gvc: Trajectory-guided generative video coding at ultra-low bitrates.
- Wiegand, T.; Sullivan, G.; Bjontegaard, G.; and Luthra, A. 2003. Overview of the h.264/avc video coding standard. *IEEE Transactions on Circuits and Systems for Video Technology* 13(7):560–576.
- Wu, Z.; Wang, Y.; Feng, M.; Xie, H.; and Mian, A. 2023. Sketch and text guided diffusion model for colored point cloud generation. In *Proceedings of the IEEE/CVF International Conference on Computer Vision*, 8929–8939.
- Xi, D.; Wang, J.; Liang, Y.; Qiu, X.; Huo, Y.; Wang, R.; Zhang, C.; and Li, X. 2025. Omnivdiff: Omni controllable video diffusion for generation and understanding. *arXiv preprint arXiv:2504.10825*.
- Yin, S.; Wu, C.; Liang, J.; Shi, J.; Li, H.; Ming, G.; and Duan, N. 2023. Dragnuwa: Fine-grained control in video generation by integrating text, image, and trajectory. *arXiv preprint arXiv:2308.08089*.
- Yin, S.; Zhang, Z.; Chen, B.; Wang, S.; and Ye, Y. 2024. Compressing scene dynamics: A generative approach.
- Zhang, Q.; Wang, Y.; Huang, L.; and Jiang, B. 2020. Fast cu partition and intra mode decision method for h. 266/vvc. *IEEE Access* 8:117539–117550.
- Zhang, C.; Liang, Y.; Qiu, X.; Yi, F.; and Li, X. 2024. Vast 1.0: A unified framework for controllable and consistent video generation. *arXiv preprint arXiv:2412.16677*.
- Zhang, P.; Li, J.; Chen, K.; Wang, M.; Xu, L.; Li, H.; Sebe, N.; Kwong, S.; and Wang, S. 2025. When video coding meets multimodal large language models: A unified paradigm for video coding.
- Zhao, M.; Wang, R.; Bao, F.; Li, C.; and Zhu, J. 2025. Controlvideo: conditional control for one-shot text-driven video editing and beyond. *Science China Information Sciences* 68(3):132107.
- Zhou, H.; Wang, C.; Nie, R.; Liu, J.; Yu, D.; Yu, Q.; and Wang, C. 2025. Trackgo: A flexible and efficient method for controllable video generation. In *Proceedings of the AAAI Conference on Artificial Intelligence*, volume 39, 10743–10751.